



Physical understanding of axonal growth patterns on grooved substrates: groove ridge crossing versus longitudinal alignment

Deming Zhang^{1,2} · Hairui Suo³ · Jin Qian⁴ · Jun Yin^{1,2}  · Jianzhong Fu^{1,2} · Yong Huang⁵

Received: 29 April 2020 / Accepted: 29 July 2020 / Published online: 11 August 2020
© Zhejiang University Press 2020

Abstract

Surface topographies such as micrometric edges and grooves have been widely used to improve neuron outgrowth. However, finding the mechanism of neuron–surface interactions on grooved substrates remains a challenge. In this work, PC12 cells and chick forebrain neurons (CFNs) were cultured on grooved and smooth polyacrylonitrile substrates. It was found that CFNs showed a tendency of growing across groove ridges; while PC12 cells were only observed to grow in the longitudinal direction of grooves. To further investigate these observations, a 3D physical model of axonal outgrowth was developed. In this model, axon shafts are simulated as elastic 3D beams, accounting for the axon outgrowth as well as the focal contacts between axons and substrates. Moreover, the bending direction of axon tips during groove ridge crossing is governed by the energy minimization principle. Our physical model predicts that axonal groove ridge crossing is contributed by the bending compliance of axons, caused by lower Young’s modulus and smaller diameters. This work will aid the understanding of the mechanisms involved in axonal alignment and elongation of neurons guided by grooved substrates, and the obtained insights can be used to enhance the design of instructive scaffolds for nerve tissue engineering and regeneration applications.

Keywords Grooved substrates · Neuron outgrowth · Axonal outgrowth model · Axonal crossing

Electronic supplementary material The online version of this article (<https://doi.org/10.1007/s42242-020-00089-1>) contains supplementary material, which is available to authorized users.

✉ Jun Yin
junyin@zju.edu.cn

- ¹ The State Key Laboratory of Fluid Power and Mechatronic Systems, School of Mechanical Engineering, Zhejiang University, Hangzhou 310028, China
- ² Key Laboratory of 3D Printing Process and Equipment of Zhejiang Province, School of Mechanical Engineering, Zhejiang University, Hangzhou 310028, China
- ³ School of Automation, Hangzhou Dianzi University, Hangzhou 310018, China
- ⁴ Key Laboratory of Soft Machines and Smart Devices of Zhejiang Province, Department of Engineering Mechanics, Zhejiang University, Hangzhou 310027, China
- ⁵ Department of Mechanical and Aerospace Engineering, University of Florida, Gainesville, FL 32611, USA

Introduction

Peripheral nerve injuries present a challenging health problem all over the world, as patients commonly experience the permanent loss of motor and sensory functions, and current treatment options remain unsatisfactory. Today, injured nerves of the peripheral nervous system (PNS) are generally treated by techniques such as conventional direct end-to-end sutures, nerve grafts or artificial nerve conduits [1–3]. Specifically, the use of artificial nerve conduits for nerve injury repair has attracted global attention in recent years [4–7]. Nerve tissue engineering scaffolds provide a permissive pathway for axonal outgrowth from proximal to distal nerve stumps and function as protective screens to prevent the infiltration of scar tissue. However, the application of these scaffolds often results in an inadequate functional recovery and is incompatible with the repair of nerve injuries with gaps greater than 15 mm [8, 9]. Over the past decade, the understanding of physical contact guidance cues that influence nerve outgrowth has been greatly expanded. These physical cues are found to control and regulate an array of cellular processes, including the adhesion, spreading,

alignment, migration, proliferation, differentiation, and outgrowth of nerve cells [10–13].

Due to the important role of physical guidance in nerve regeneration processes, various approaches to provide contact guidance cues have been developed. These, for example, include surface roughness, grooved textures [7], micro-sized pillars [14, 15], flexible gold nanocone arrays [16], multichannels [17], and nanofibers [18]. In particular, surface topographies with micrometric edges and grooves have been widely used to improve neuronal alignment and to accelerate longitudinal outgrowth. For example, a study by Li et al. found that dorsal root ganglion (DRG) neurons showed an increase in length and enhanced longitudinal alignment when cultured on micro-patterned poly(lactic-co-glycolic acid) (PLGA) films [19]. The physical contact guidance provided by grooved textures facilitates axonal elongation along groove edges and hence causes neuronal polarization [20, 21].

In the past, several studies have been focused on investigating the interactions between axons and micro-grooved surfaces in regards to their effect on axonal length and orientation [10, 16, 22, 23]. It is known that the axonal response may vary depending on the selected type of neuron, the substrate topography, and the size of applied topographical features [24–26]. In a study by Chua et al., primary murine neural progenitor cells (mNPCs) were cultured on PDMS substrates with a groove width of 2 μm and groove heights of 0.35, 0.8, 2, or 4 μm to investigate the effect of feature dimension on neuronal contact guidance [27]. The results indicated that both axon length and axon alignment of cultured mNPCs increase with a rise in topography depth. It was also noted that axons were more likely to grow along the grooves in contrast to bridging grooves as topography depth was increased. Nevertheless, neurons have been found to cross neighboring ridges of grooves wider than 20 μm [19, 25, 27–29]. On the basis of previous studies, it is indisputable that the mechanical interactions between neurons and surface substrates play a significant role in neuronal outgrowth. However, the mechanisms underlying the observed neuronal responses to topographical stimuli based on neuron-surface interactions are still not fully understood. Developing a comprehensive understanding of the relationship between axons and grooved substrates presents an essential step in the formation of rational strategies aimed to accelerate neuronal outgrowth after injury and disease.

The aim of this study was to investigate the physical mechanisms which dictate the guidance of axonal outgrowth on grooved topographies. For this purpose, a continuum mechanics-based model was developed to capture axonal behaviors on substrates with distinct micro-groove patterns. In this model, axonal outgrowth and focal contacts between axons and substrates were considered. The bending direction of axon tips was set to be governed by the energy

minimization principle in order to prevent detachment of axons from their corresponding substrates. Pheochromocytoma 12 (PC12) cells and chick forebrain neurons (CFNs) have been widely used as neuron cell model in neurobiological investigations [30–34], and to evaluate surface topographies effects on neurite outgrowth [4, 7, 35–37]. To validate the developed numerical model, PC12 cells and CFNs were cultured in vitro on substrates with different grooved textures. The resulting observations of PC12 axonal length and orientation showed a broad agreement with data obtained from the numerical model, which confirmed its validity. During in vitro tests, PC12 cells and CFNs were seen to show distinct responses when exposed to identical groove textures. CFNs showed a tendency to link adjacent groove ridges by growing across grooves. In contrast, PC12 cells were seen to remain within the same groove bottom or ridge while elongating in parallel with the grooves. In explaining such distinct phenomena of axonal groove crossing for different neuron types, our model implies that the Young's modulus as well as the diameter of axons play leading roles in axonal outgrowth, and hence, determine whether elongation takes place in parallel or perpendicular to the grooves. This work will further our understanding of the effects grooved substrates have on axonal alignment and elongation. Consequently, it may lead to the design of improved instructive scaffolds for tissue engineering applications and nerve tissue regeneration.

Experimental methods

Topographical characterization of grooved substrates

Grooved polyacrylonitrile (PAN) substrates were fabricated with an inner grooved spinneret using the dry-jet wet spinning method, as introduced in our previous work [4, 7]. The constructed topographical substrates had a groove height of $\sim 120 \mu\text{m}$ and groove widths of either ~ 183 or $\sim 349 \mu\text{m}$, as shown in Fig. 1A. Smooth PAN substrates were fabricated based on the use of a smooth spinneret. Optical microscopy (Nikon AZ100, Japan) was applied to evaluate the structures of constructed grooved substrates. Groove textures were characterized according to the average groove height (height from groove top to bottom, $2H$), the average groove width (distance between two neighboring groove tops, W) and the average ridge width (width at $2/3$ groove height). As shown in Fig. 1B, the grooved texture can be described by

$$y = H \cdot \sin\left(\frac{2\pi}{W}x\right). \quad (1)$$

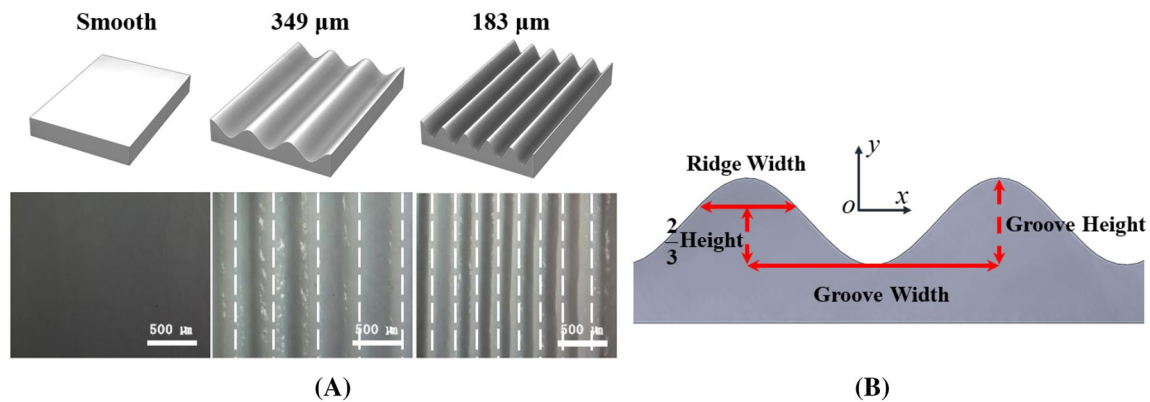


Fig. 1 **A** Microscope images of smooth and grooved substrates. White dotted lines represent the top of ridges. **B** Definition of groove width, ridge width, and groove height

Table 1 Geometry of the grooved substrates

	Large groove	Small groove
Groove width (μm)	349.2 ± 6.6	182.8 ± 6.1
Groove height (μm)	120.2 ± 6.1	119.0 ± 14
Substrate texture (μm)	$y = 60 \times \sin(0.018x)$	$y = 60 \times \sin(0.034x)$

The geometry of the generated grooved substrates with different textures is summarized in Table 1.

In vitro neuron culture on grooved substrates

PC12 cells were obtained from the Cell Bank of the Chinese Academy of Sciences (Shanghai, China). The cells were cultured in Dulbecco's Modified Eagle medium (DMEM; HyClone, USA), which was supplemented with 10% fetal bovine serum (FBS; Gibco, USA) and 1% penicillin/streptomycin (Aladdin, China). Cells were incubated at 37 °C with 5% CO₂ for 120 h. PC12 cells were harvested from cell culture dishes at a concentration of 8×10^4 cells/mL and loaded onto the fabricated substrates with smooth and grooved textures.

Chick forebrain neurons (CFNs) were harvested from cerebral hemispheres of 7- to 8-day-old chick embryos (dissected and cleared of meningeal membranes). The forebrain was separated as described by Pettmann et al. [38] and dissociated using a nylon sieve. Cells were collected and cultured at a concentration of 1×10^4 cells/mL in M199 culture medium (HyClone, USA) supplemented with 10% FBS (Gibco, USA), 1% B27 (Gibco, US), 100 ng/mL β -NGF (Biovision, USA), and 1% penicillin/streptomycin (Aladdin, China). The obtained cell suspension was loaded onto the fabricated smooth and grooved substrates.

After incubation for 24, 72, and 120 h, the substrates were rinsed with phosphate-buffered saline (PBS, Solarbio, China) and then incubated in 1 $\mu\text{g}/\text{mL}$ calcein acetoxymethyl ester

(Calcein-AM; Aladdin, China) and 5 $\mu\text{g}/\text{mL}$ propidium iodide (PI; Aladdin, China) for 30 min to remove unattached cells. The samples were stained with 1 $\mu\text{g}/\text{mL}$ Calcein-AM and 2 $\mu\text{g}/\text{mL}$ PI for 30 min. Following this, they were again rinsed with PBS and covered with glass coverslips. Images were taken using an inverted fluorescence microscope (Nikon Tis, Japan). The outgrowth characteristics and morphology of PC12 cells and CFNs were analyzed using ImageJ (v1.51, USA National Institutes of Health).

Measurement of axon stiffness

Nanoindentation tests were performed using a nanoindenter (G200, Agilent, USA) to characterize the stiffness of PC12 cells and CFNs [39, 40]. During nanoindentation, the indenter tip (spherical indenter) on the cantilever was set at the central region of axons, and a constant downward displacement rate of 5 nm/s was applied until an indentation depth of 10 nm was reached. For each specimen, 10 indentations were carried out.

Once the loading force–displacement data of axon indentation were obtained, the Hertz model was utilized to evaluate the Young's modulus of axons [41, 42]. Here, the loading force–indentation curves were fitted over an initial 15% indentation depth. The relationship between the indentation δ and the loading force F is described by the Hertz model as

$$F = \frac{4\sqrt{R}}{3} E^* \delta^{\frac{3}{2}} \quad (2)$$

where R is the radius of the nanoindentation tip. E^* is the effective modulus of the tip-sample system and is calculated as

$$\frac{1}{E^*} = \frac{1 - \nu^2}{E} + \frac{1 - \nu_i^2}{E_i} \quad (3)$$

where E , ν and E_i , ν_i represent the Young's modulus and the Poisson's ratio for the axon and the nanoindentation tip,

respectively. In this description, the effective modulus of the tip-sample system is mainly contributed by the softer one [43, 44]. Since the indenter tip is significantly stiffer than the axon ($E_t \gg E$) here, the Young’s modulus of the axon can be estimated based on Eqs. (2) and (3) as

$$E = \frac{3(1 - \nu^2)}{4\sqrt{R}} \cdot \frac{F}{\delta^{\frac{3}{2}}} \tag{4}$$

Statistical analysis

In the statistical analysis, at least six independent nanoindentation tests were performed for different neuron types, and only data obtained for axons with a length of $L_{Axon} > 5 \mu\text{m}$ were included. For each topographical feature, the presented data account for the average of six cell culture plates. Unless otherwise stated, all characterizations were performed using data analysis software SPSS 18.0 (IBM, USA). All data were presented in the form of mean \pm standard deviation. Statistical significance ($*p < 0.05$, $**p < 0.01$) was determined using Bonferroni’s multiple comparison one-way ANOVA.

Physical model of axonal outgrowth on grooved substrates

A 3D physical model was developed to investigate the effect of grooved substrates on axonal outgrowth. This model takes into consideration several factors, including axon tip outgrowth, traction forces at the axon tip, and adhesion forces between axon and substrate. To numerically model the process of axon outgrowth, the following assumptions were made.

- (a) Axons can be modeled as 3D solid cylinders with a constant diameter.
- (b) The axonal motion is quasi-static [45].

- (c) The substrate is rigid. The Young’s modulus of PAN substrates is $\sim 50 \text{ MPa}$ [46]. This is considerably higher than the Young’s modulus observed for axons of PC12 cells and CFNs (~ 1 to 5 kPa). For this reason, the utilized polymeric substrate is generally treated as rigid [47].
- (d) Axons can be modeled as an elastic material, as seen in previous work. Dennerll et al. [48] found that neurites adopt an elastic behavior when they are stretched for a short period of time (3 min).
- (e) The axon always attaches to the substrate surface during outgrowth. Therefore, the traction force at the axon tip is exerted onto the tangent planar surface of the grooved substrate, and the axon-substrate adhesion force is applied in the normal direction of the tangent planar surface (Fig. 2).

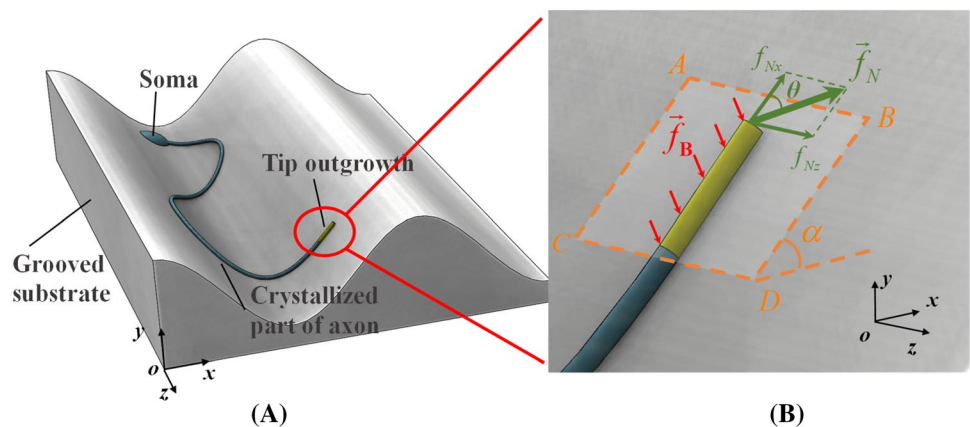
Axon tip outgrowth and crystallization

Axonal outgrowth in this model is divided into two parts, namely tip outgrowth and crystallization. Axons show an elastic elongation when traction forces are applied to the axon tip. Additionally, an inelastic elongation at the tip of axons is induced as tubulin molecules are added to the end of the rod-like microtubules. The assembly of tubulin molecules into microtubules contributes to the elongation of axons [49, 50]. In this model, elastic elongation is determined by the elasticity of growth cones, while inelastic elongation is triggered when traction forces exceed a tension force threshold at the axon tip [51]. Thus, the tip outgrowth rate $\frac{dl_t}{dt}$ is described as

$$\frac{dl_t}{dt} = k_t \left(\|\vec{f}_N\| - F_0 \right) \tag{5}$$

where \vec{f}_N represents the traction force exerted at the tip of the axon, l_t is the inelastic elongation length, k_t represents the tip outgrowth rate coefficient and F_0 is the tension force

Fig. 2 Schematic of axonal outgrowth on a grooved substrate and force distribution at the axon tip. The yellow fraction at the tip of the axon represents the distal growing part. The blue fraction represents the proximal part of the axon which is crystallized in the model



threshold required to trigger tip outgrowth [50]. For axons of PC12 cells, the tension force threshold for inelastic elongation has been reported as ~ 1 nN [52], while CFNs have been shown to exhibit a lower tension force threshold of ~ 50 pN [53]. Since only the distal part of axons stretches during outgrowth, the proximal part of axons is artificially crystallized in the model. All parameters applied for the tip outgrowth model are listed in Table 2. The Young’s modulus and Poisson’s ratio (Poisson’s Ratio $\nu = 0.45$ [54, 55]) were used as material parameters for axons, and the linear elasticity of axon was used in all finite element simulations.

Traction force at the axon tip

During axonal outgrowth, the growth cone represents the motile apparatus of neurons. This dynamic extension is a highly sensitive structure at the axon tip [59, 60], which plays an active role in the elongation and branching of a developing axon. The binding between growth cone and substrate leads to the formation of a complex that mechanically couples receptors and actin filaments (F-actin). This enables the generation of traction forces in the axon tip [61, 62]. The relationship between traction forces and tip outgrowth rates is largely dependent on the selected type of neuron. Due to the complex morphology and dynamic behavior of the growth cone, the traction force exerted at the tip of the axon is generally modeled as a random force [51, 63]. Based on Assumption (e), the traction force \vec{f}_N is exerted onto the tangential plane of the grooved texture (S_{ABCD} in Fig. 2B) as

$$f_{Nx} = \|\vec{f}_N\| \cdot \cos\theta \text{ and } f_{Nz} = \|\vec{f}_N\| \cdot \sin\theta \tag{6}$$

where f_{Nx} and f_{Nz} are the components of \vec{f}_N in the x - and z -directions, respectively, and $\theta \in [0, \pi]$ is a random angle which describes the orientation of axonal outgrowth.

Adhesion between axon and substrate

Adhesion forces play a significant role in anchoring axons to the extracellular matrix (ECM) and allow for the transmission of mechanical signals between these two segments [47]. For this reason, the adhesion between axons and substrates is considered in this model. A previous experimental study by Aeschlimann et al. [45] indicated that the adhesion force per unit area between the growth cone and the substrate is maintained at a constant value of ~ 0.1–0.2 kPa. Therefore, the neuron-substrate adhesion force \vec{f}_B is set to be constant in this model. This is applied in the normal direction of the tangent plane surface S_{ABCD} (Assumption e), as shown in Fig. 2.

Axonal groove crossing

Since the axon is assumed to consistently attach to the substrate during outgrowth (Assumption e), the behavior of the axon tip at the top of the groove ridge has to be modeled carefully. The distance between the axon tip and the substrate (l_{Bond}) is recalculated in each step to determine whether the axon remains attached to the substrate. If $l_{Bond} \leq \eta$, the axonal extension follows its previous direction to cross the groove ridge (Fig. 3B). This prediction is based on the assumption that the axon tip attaches to the substrate when $l_{Bond} \leq \eta$. Furthermore, η presents a considerably small distance threshold. When $l_{Bond} > \eta$, the axon tip is assumed to detach from the substrate. In this model, the direction of axonal extension is governed by the energy minimization principle to ensure axonal substrate attachment during outgrowth, as described in Assumption (e). As shown in Fig. 3C, the axonal growing direction θ is updated in every iteration by adding $\Delta\theta$ ($\Delta\theta \in [0, \frac{\pi}{18}]$) until $l_{Bond} \leq \eta$. Thus, the bending direction of the axon tip changes in order to adapt to the groove’s slope.

Table 2 Parameters and their corresponding values in the physical model

Parameter	Definition	Values		References
		CFNs	PC12 cell	
D (μm)	Diameter	4 ± 0.51	6 ± 0.62	Immunofluorescence stained images
E (kPa)	Young’s modulus	1.47 ± 0.48	4.43 ± 0.88	Nanoindentation testing
ν	Poisson’s Ratio	0.45	0.45	[54, 55]
f_N (nN)	Magnitude of force exerted on the tip of axon	0.45	10	[56, 57]
F_0 (nN)	The tension force threshold	0.05	1	[52, 53]
f_B ($\mu\text{dyne}/\mu\text{m}^2$)	The adhesion force per unit area	20	20	[45]
μ_1 (Pa s)	The first constant of friction	10^4	10^4	[58]
$\frac{dl}{dt}$ ($\mu\text{m}/\text{h}$)	Inelastic elongation rate	2.8	1.4	Immunofluorescence stained images
$\frac{dl_{cr}}{dt}$ ($\mu\text{m}/\text{h}$)	Crystallization rate	2.8	1.4	Immunofluorescence stained images
η (μm)	Distance threshold	10^{-2}	10^{-2}	[47]

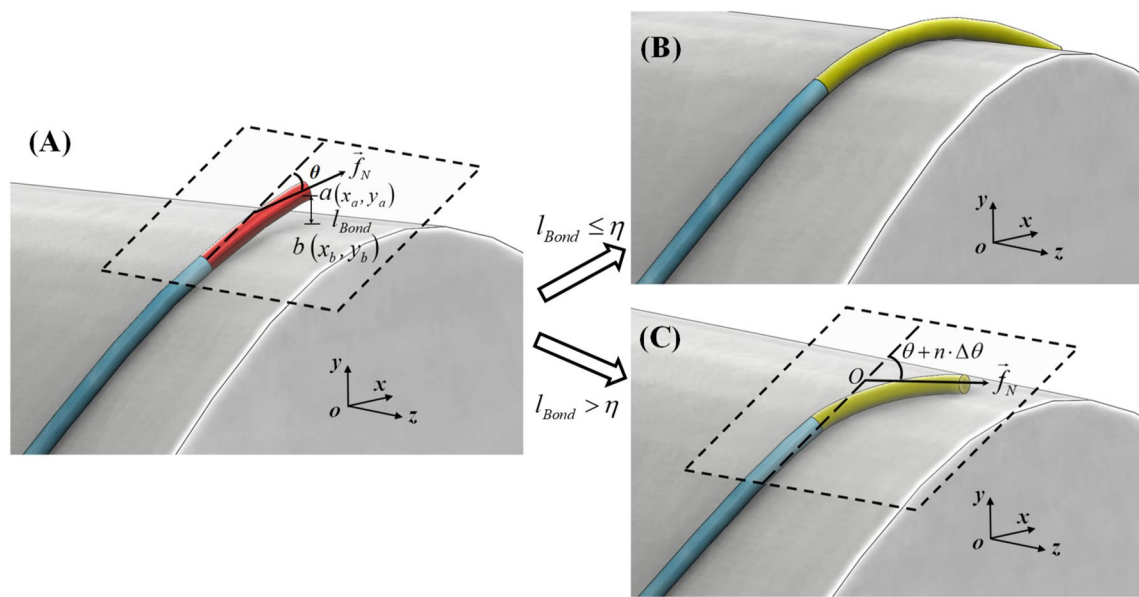


Fig. 3 Presentation of the bending energy minimization process for axons extending across the ridge of a grooved substrate. **A** Detachment of the axon tip (red) from the groove ridge with a distance of l_{Bond} . **B** If $l_{\text{Bond}} \leq \eta$, the growing axon will maintain its previous

direction as it extends; however, **C** if $l_{\text{Bond}} > \eta$, the growing axon will change the direction of extension to ensure firm attachment of the axon tip (yellow) to the substrate

Using the commercial finite element software package ABAQUS, simulations were carried out with different initial locations and orientations of the axon to obtain a favorable statistical average of axon behavior. Axon traction forces (Fig. 2) and crystallizations were incorporated in the framework of the script language Python and by applying a user-defined element (UEL).

Results

PC12 cell outgrowth and model validation

In this work, PC12 cells were cultured on smooth and grooved PAN substrates, where grooved substrates provided a groove width of either 183 or 349 μm (Fig. 4B). During 120 h in culture, PC12 cells displayed typical neuronal characteristics, namely prominent cell soma with two neurites. To quantitatively describe the morphology and directional outgrowth of PC12 cells, the definitions of axon length (L_{Axon}), axon diameter (D_{Axon}), and axon outgrowth orientation ($\theta_{\text{Orientation}}$) are illustrated in Fig. 4A. On smooth substrates, PC12 cells were not found to grow in specified directions, and no predominant orientation of axons was observed within 120 h of culture. Contrary, PC12 cells cultured on grooved substrates grew freely and developed very short axons within the first 24 h. After 72 h, PC12 cells showed an increase in morphological alignment as their axons reached a length which enabled sensing of the physical constraint

provided by the groove wall. Interestingly, it was noted that all PC12 cells remained within the same groove bottom or ridge (Fig. 4B). As seen in Fig. 5A, the axon length of PC12 cells increased from ~ 35 to $\sim 100 \mu\text{m}$ on all grooved substrates between 24 and 120 h of culture. After 120 h in culture, PC12 cells showed average axonal lengths of 97.3 and 105.2 μm on 349 and 183 μm wide grooves, respectively. Hence, a decrease in groove width was shown to correlate with increased axonal length. Additionally, a decrease in groove width was observed to correspond to improved PC12 alignment. This trend was seen after a culture time of 72 h (Fig. 5B). Based on the discussed results, it is apparent that the grooved texture of substrates significantly impacts the morphology and outgrowth of PC12 cells.

The numerical simulation was also applied to quantitatively understand the influence of grooved textures on axon outgrowth. Parameters utilized for this model are listed in Table 2, and the derived numerical results representing axonal outgrowth on smooth and grooved substrates are illustrated in Fig. 5. It can be noted that the obtained numerical values of axon length and orientation are in strong agreement with the experimental results of the in vitro PC12 cell culture. This confirms the sufficient accuracy of our physical model.

Axonal groove crossing

CFNs were cultured on grooved substrates with a groove width of 183 μm . The obtained data were utilized to contrast

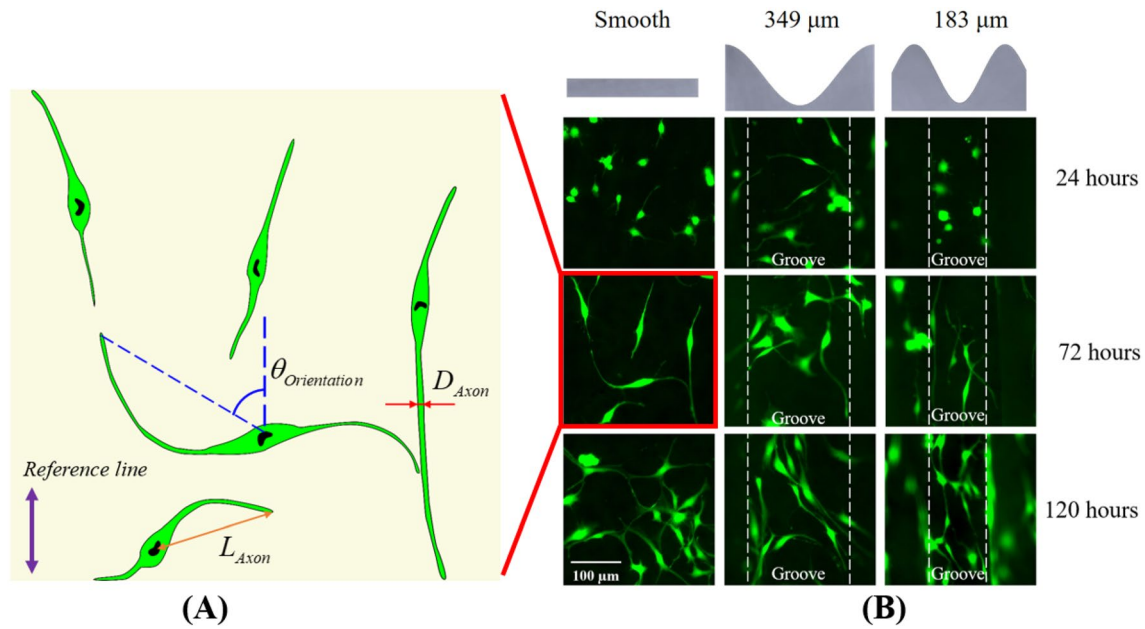


Fig. 4 **A** Definition of the length, orientation, and diameter of neurites. The distance from the center of the soma to the end of the axon (orange line) represents the length of the axon (L_{Axon}). The projection width of the axon (red line) is defined as the diameter of the

axon (D_{Axon}). The angle of neurite outgrowth (blue dash line) represents the axon orientation ($\theta_{Orientation}$). **B** Immunofluorescent images of PC12 cells cultured on substrates with different surface textures. Scale bar represents 100 μm

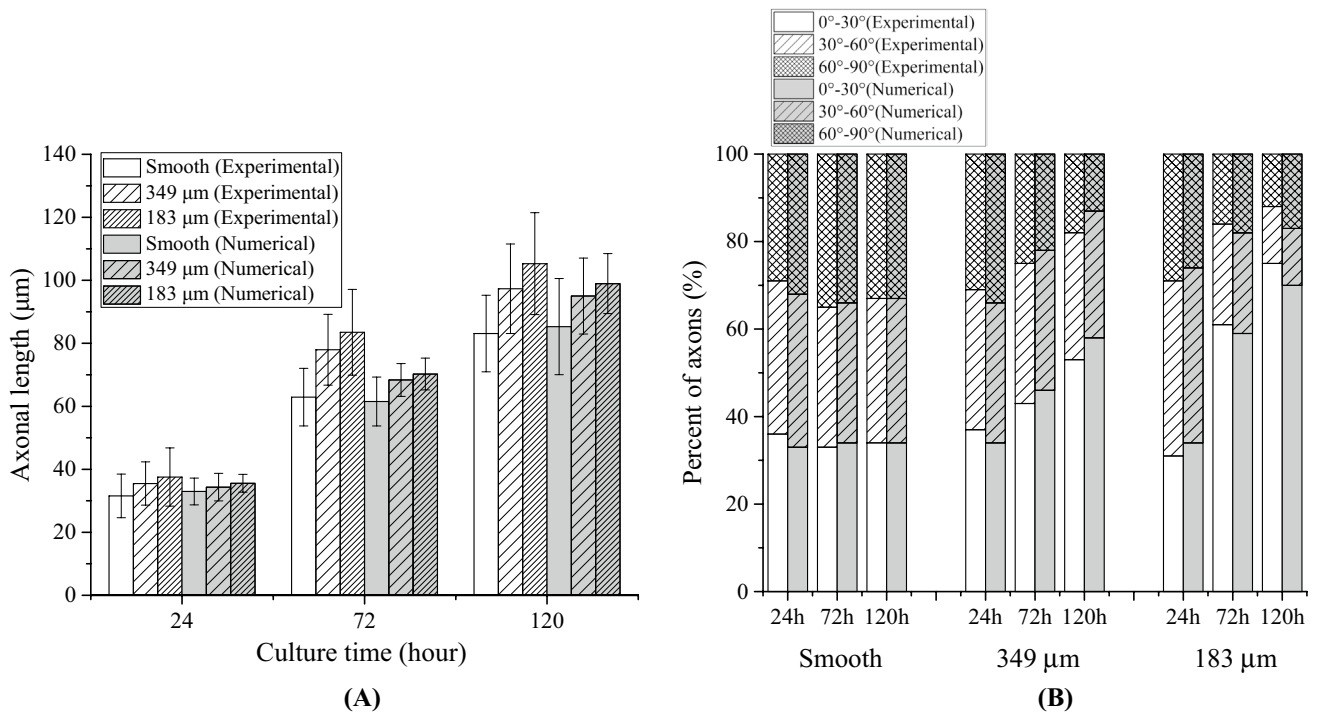


Fig. 5 The axonal length **A** and orientation **B** of PC12 cells grown on substrates with smooth surfaces, 349 μm wide grooves and 183 μm wide grooves after 24, 72 and 120 h in culture

the response of different neuron types to varying substrate textures. It was observed that the axonal length of CFNs was largely increased compared to PC12 cells (Fig. 6). A significant observation was represented by the growth pattern of CFNs and PC12 cells. Interestingly, it was noted that CFN axons showed a preferred growth extension across groove ridges (Fig. 6B). In contrast, PC12 cells were seen to exclusively grow along grooves and remained within the same groove structures for the entire culturing period (Fig. 6A). Hence, PC12 cells appeared to be effectively guided by surface topographical features, while CFNs disregarded topographical obstacles to cross groove ridges.

The developed physical axon outgrowth model allowed for an investigation into the different responses observed for PC12 cells and CFNs when exposed to identical grooved textures. The Young's modulus of PC12 cells was found to be twice as large as the Young's modulus of CFNs (Table 2). For this reason, the effect of axonal stiffness on growth patterns of axons cultured on 183 μm wide grooves was numerically modeled. As shown in Fig. 7A, when the Young's modulus of axons with a diameter of 4 μm is increased from 1.5 to 5 kPa, the probability of axonal groove crossing is significantly decreased. It was further identified that axons with their Young's modulus < 2 kPa show a consistent ability to cross groove ridges (Fig. 7A). On the other hand, axons with their Young's modulus > 5 kPa were seen to bend toward the longitudinal direction of grooves and grow in parallel with neighboring ridges.

The axon diameter is another important factor which has been reported to effectively regulate axon outgrowth [25].

For this reason, the developed physical model was utilized to investigate this factor and its impact on axonal outgrowth on grooved substrates. Here, axons with varying diameters between 3 and 6 μm were simulated at a constant Young's modulus of 1.47 kPa. The numerical results showed that the probability of axonal groove crossing decreases with an increase in the axon diameter. Interestingly, axons showed a consistent ability to cross groove ridges if their diameter was lower than 4 μm (Fig. 7B). As previously described, the Young's modulus of PC12 cells and CFNs measured by nanoindentation equaled 4.4 ± 0.88 and 1.48 ± 0.48 kPa, respectively, and the diameter of PC12 cells and CFNs was found to be ~ 6 and ~ 4 μm , respectively (Fig. 4). Taking this into consideration, the numerical model predicts a higher probability of axonal groove crossing for CFNs compared to PC12 cells. This is in strong alignment with the experimental results obtained from in vitro cultures of CFNs and PC12 cells (Fig. 6).

Discussion

Topographical features are known to influence the morphology and outgrowth of neurons. Our previous work [7, 51] have demonstrated that substrates with groove width from about 50–350 μm could affect the axonal morphologies, orientation, and growth behaviors. In the present study, PC12 cells and CFNs were shown to display distinct responses when subjected to microgrooves. Here, CFNs showed the ability to link adjacent ridges by growing across grooves.

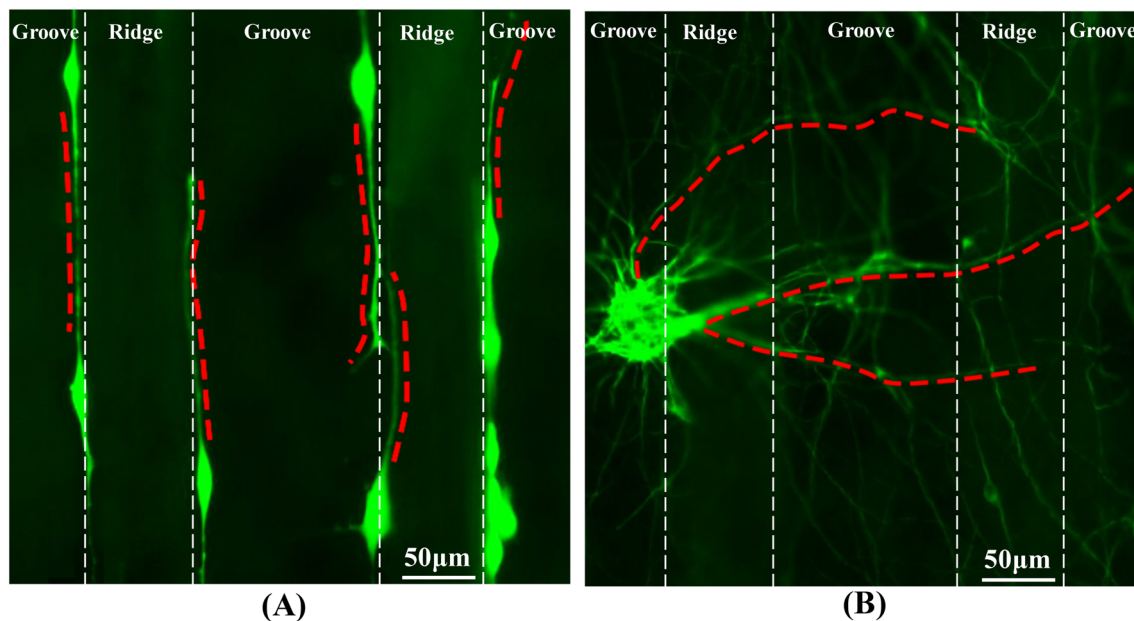


Fig. 6 Immunofluorescent images of PC12 cells and CFNs cultured on substrates with 183 μm wide grooves after 168 h in culture. Red dashed lines mark axon outlines. **A** PC12 cells aligned with groove structures. **B** CFNs extended across groove ridges

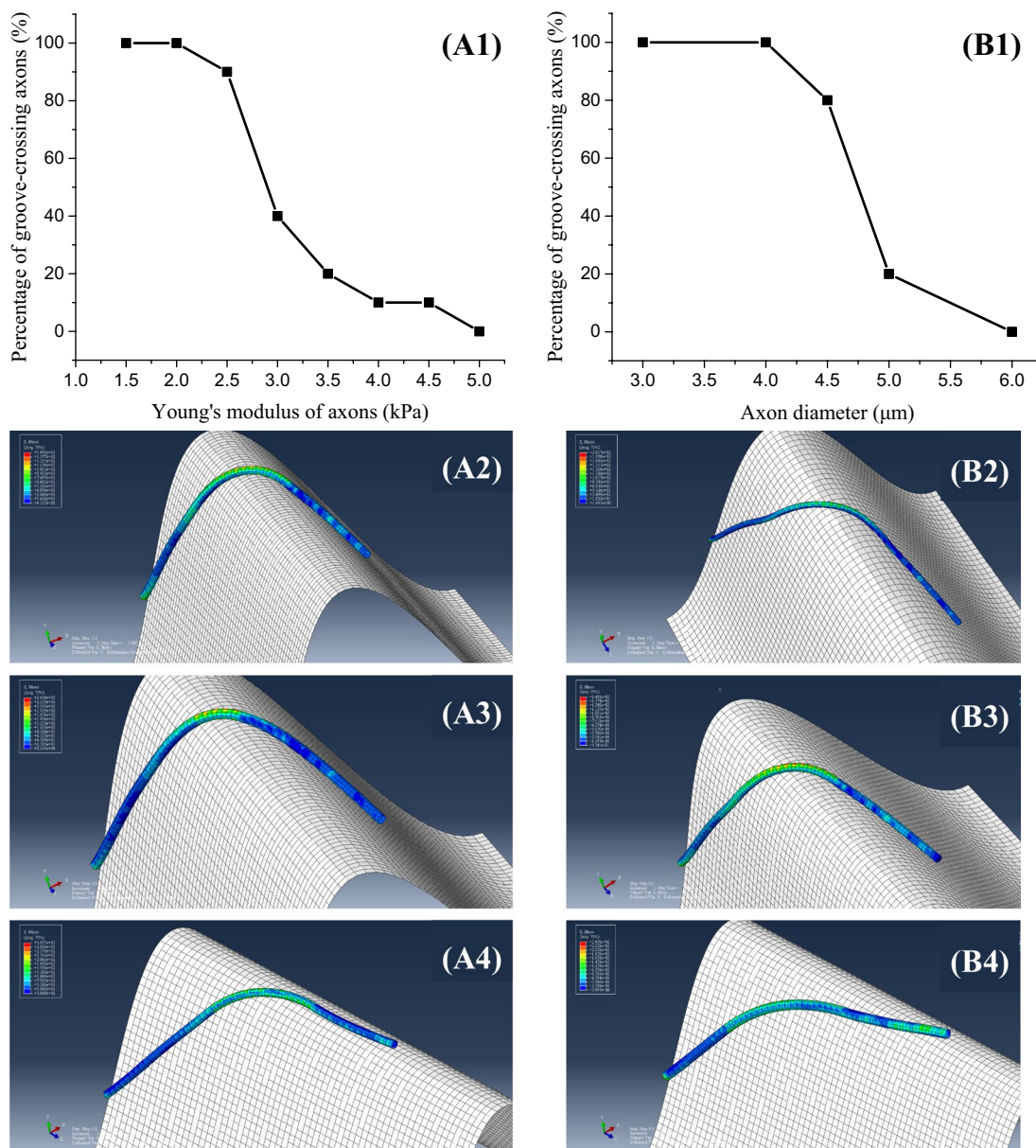


Fig. 7 Effect of axonal Young's modulus and diameter on groove-guided axon outgrowth patterns. **A1** Percentage of groove-crossing axons plotted against the axonal Young's modulus (axon diameter = 4 μm, and $n = 15$). Axonal growth patterns on groove ridge when axonal Young's modulus equals to 2 kPa (**A2**), 2.5 kPa (**A3**) and

4 kPa (**A4**). **B1** Percentage of groove-crossing axons plotted against the axon diameter (Young's modulus = 1.48 kPa, and $n = 15$). Axonal growth patterns on groove ridge when axonal diameter is 3 μm (**B2**), 4 μm (**B3**) and 5 μm (**B4**)

This was not observed for PC12 cells which instead showed the tendency to grow along grooves. The axonal outgrowth model developed in this work is the first recorded numerical model that quantitatively predicts axonal 3D outgrowth on grooved substrates. As shown in this study, the numerical model was able to predict the observed responses of CFNs and PC12 cells to groove ridges. Generally, neurons are soft materials with nonlinear constitutive laws [64]. But, it has to be noticed that the average deformation of PC12 cells and

CFNs during outgrowth on the grooved substrate is less than 5%. Thus, we assumed that C12 cells and CFNs are linear elastic materials within the small deformation region. The similar assumption was also proposed in previous models of neural deformation [45].

In the model, the adhesion between axons and substrates was taken into account. Furthermore, axons were assumed to always attach to the substrate during axonal outgrowth. The primary site of cellular adhesion to substrates is represented

by focal adhesions which link the extracellular matrix to the cytoskeleton of adhered cells [65]. This allows for the transmission of mechanical signals between intracellular actomyosin networks and the corresponding substrates [66]. When the axon tip grows perpendicular to substrate grooves and hence crosses groove ridges, it is required to bend downward in order to prevent detachment from the substrate (Fig. 8A). To investigate the deformation of axon tips during the groove-crossing process, a cantilever beam with the angle deflection β was applied (Fig. 8B). Here, the axon tip was simplified as a cantilever beam with the Young’s modulus E and the moment of inertia I (Fig. 8B). The adhesion force was simplified as a uniform load distribution f_b per unit length. Thus, the adhesion force required to keep the axon attached to the substrate corresponds to [67, 68].

$$f_b = \frac{6EI\beta}{l^3} \tag{7}$$

where l describes the length of the growing axon without crystallization. Moreover, the bending energy of the axon tip during groove crossing can be described as (Supplementary material)

$$W_B = \frac{9EI\beta}{10l} \tag{8}$$

The adhesion energy between the axon and substrate is described as W_A . W_A summarizes the collective bonding energy of focal contacts between a cell and the extracellular matrix [69]. If $W_A \geq W_B$, the level of adhesion energy is sufficient to maintain attachment of the axon tip to the substrate as the axon crosses the ridge while following its initial direction (Fig. 3B). Contrary, if $W_A < W_B$, the level of adhesion energy is not sufficient to maintain attachment of the axon and hence disfavors bending of the axon tip through the groove ridge. As a result, the axon tip is forced to change its direction of extension. This reduces the required bending energy (W_B) and hence allows for the axon to remain

attached to the substrate under the given adhesion energy (W_A ; Fig. 3C).

As shown in Eq. (8), the bending energy of the axon tip is proportional to the axonal Young’s modulus, the axon diameter and the angle deflection. Both the Young’s modulus (1.47 kPa) and the diameter (4 μm) of CFN axons were shown to be smaller than the corresponding values observed for PC12 cells (4.43 kPa, 6 μm). For this reason, a larger bending energy is required for PC12 cells, compared to CFNs, to cross the same groove ridge. Importantly, the adhesion energy between axons and substrates does not vary significantly between different neuron types [47]. Consequently, the adhesion energy of CFN axons exceeds the bending energy during groove ridge crossing, whereas the bending energy of PC12 axons is too large to be overcome by the given adhesion energy. This provides a physical explanation for the distinction between the observed growth patterns of the two cell types (Fig. 6). Finally, it should be noted that the physical model developed as part of this study is based on the assumption that axons can be treated as a homogenous elastic material (Assumptions a, d). This simplification provides a basis to elucidate the physical processes underlying observed cellular behaviors. Nevertheless, it should be taken into consideration that axons present complex structures, which can exhibit inhomogeneous and anisotropic responses [47].

Conclusions

This work aims to investigate the effects of grooved substrates on the axonal outgrowth of different neuron types. Based on an in vitro culture, it was found that the axonal alignment and longitudinal elongation of PC12 cells can be modulated by decreasing the groove width of the substrate. More importantly, PC12 cells and CFNs showed distinct responses when exposed to similar grooved textures: CFNs were found to link adjacent grooves by growing across the ridges, whereas PC12 cells consistently grew along the

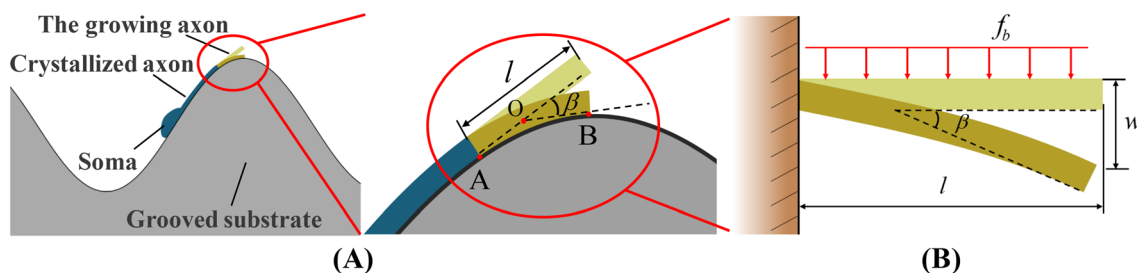


Fig. 8 Schematic of axon outgrowth on a grooved substrate. **A** The proximal part of the axon (blue) is firmly attached to the substrate and crystallized in the model. The distal part of the axon (light yellow) extends into its initial direction. Due to adhesion forces between the

axon and its substrate, the distal part of the growing axon is deformed and attaches to the substrate (dark yellow). **B** Simplified cantilever beam with a uniform cross-section which carries a uniformly distributed load f_b per unit length

grooves while remaining in their initial groove bottom. In addition to the *in vitro* culture, a 3D physical model of axonal outgrowth was developed. Based on the developed model, it was revealed that the Young's modulus and diameter of axons play the leading roles in determining the growth pattern of extending axons on grooved substrates, consistent with the experimental observations on PC12 cells and CFNs. This work will aid the understanding of the underlying mechanisms that govern axonal alignment and elongation of neurons on grooved substrates. Hence, it is aimed to promote the development of improved instructive scaffolds for nerve tissue regeneration.

Acknowledgements This study was partially supported by the National Key Research and Development Program of China (Grant No. 2018YFA0703000), the Key Research and Development Program of Zhejiang Province (Grant No. 2017C01063), the Science Fund for Creative Research Groups of the National Natural Science Foundation of China (Grant No. 51821093), the National Natural Science Foundation of China (Grant Nos. U1609207, 11672268), ZJU Scholarship for Outstanding Doctoral Candidates and Scholarship Program supported by China Scholarship Council (No. 201906320187).

Author Contributions Deming Zhang carried out the numerical simulations and drafted the manuscript. Hairui Suo performed *in vitro* cell outgrowth and experimental data analysis. Jin Qian worked on the nanoindentation tests and revised the manuscript. Jun Yin is the principal investigator, designed the numerical model, organized, and revised the manuscript. Yong Huang and Jianzhong Fu helped to revise the manuscript, and coordinate the study.

Compliance with ethical standards

Conflict of interest Deming Zhang, Hairui Suo, Jin Qian, Jun Yin, Jianzhong Fu, and Yong Huang declare that they have no conflict of interest.

Ethical approval This article does not contain any studies with human or animal subjects performed by any of the authors.

References

- Palispis WA, Gupta R (2017) Surgical repair in humans after traumatic nerve injury provides limited functional neural regeneration in adults. *Exp Neurol* 290:106–114
- Narayan SK, Arumugam M, Chittoria R (2019) Outcome of human peripheral nerve repair interventions using conduits: a systematic review. *J Neurol Sci* 396:18–24
- Singh A, Shiekh PA, Das M, Seppala J, Kumar A (2019) Aligned chitosan-gelatin cryogel-filled polyurethane nerve guidance channel for neural tissue engineering: fabrication, characterization, and *in vitro* evaluation. *Biomacromolecules* 20:662–673
- Yin J, Wang ZH, Chai WX, Dai GL, Suo HR, Zhang N, Wen XJ, Huang Y (2017) Fabrication of inner grooved hollow fiber membranes using microstructured spinneret for nerve regeneration. *J Manufact Sci Eng Trans Asme* 139:111007
- Zhou C, Liu B, Huang Y, Zeng X, You HJ, Li J, Zhang YG (2017) The effect of four types of artificial nerve graft structures on the repair of 10-mm rat sciatic nerve gap. *J Biomed Mater Res Part A* 105:3077–3085
- Singh A, Asikainen S, Teotia AK, Shiekh PA, Huotilainen E, Qayoom I, Partanen J, Seppala J, Kumar A (2018) Biomimetic photocurable three-dimensional printed nerve guidance channels with aligned cryomatrix lumen for peripheral nerve regeneration. *ACS Appl Mater Interfaces* 10:43327–43342
- Suo HR, Wang ZH, Dai GL, Fu JZ, Yin J, Chang LQ (2018) Polyacrylonitrile nerve conduits with inner longitudinal grooved textures to enhance neuron directional outgrowth. *J Microelectromech Syst* 27:457–463
- Isaacs J, Browne T (2014) Overcoming short gaps in peripheral nerve repair: conduits and human acellular nerve allograft. *Hand* 9:131–137
- Hopkins TM, Little KJ, Vennemeyer JJ, Triozzi JL, Turgeon MK, Heilman AM, Minter D, Marra K, Hom DB, Pixley SK (2017) Short and long gap peripheral nerve repair with magnesium metal filaments. *J Biomed Mater Res Part A* 105:3148–3158
- Zhang Q, Li YL, Sun H, Zeng L, Li X, Yuan B, Ning CY, Dong H, Chen XF (2015) hMSCs bridging across micro-patterned grooves. *RSC Adv* 5:47975–47982
- Zhang DT, Wu S, Feng JY, Duan YY, Xing DM, Gao CY (2018) Micropatterned biodegradable polyesters clicked with CQAASIKVAV promote cell alignment, directional migration, and neurite outgrowth. *Acta Biomater* 74:143–155
- Park S, Choi KS, Kim D, Kim W, Lee D, Kim HN, Hyun H, Lim KT, Kim JW, Kim YR, Kim J (2018) Controlled extracellular topographical and chemical cues for acceleration of neuronal development. *J Ind Eng Chem* 61:65–70
- Krishnamoorthy S, Zhang ZY, Xu CX (2020) Guided cell migration on a graded micropillar substrate. *Bio-Des Manuf* 3:60–70
- Wang B, Shi J, Wei J, Wang L, Tu XL, Tang YD, Chen Y (2017) Fabrication of elastomer pillar arrays with height gradient for cell culture studies. *Microelectron Eng* 175:50–55
- Wei J, Pozzi D, Severino FPU, Torre V, Chen Y (2017) Fabrication of PLGA nanofibers on PDMS micropillars for neuron culture studies. *Microelectron Eng* 175:67–72
- Toma M, Belu A, Mayer D, Offenhäusser A (2017) Flexible gold nanocone array surfaces as a tool for regulating neuronal behavior. *Small* 13(24):1700629
- Yao L, de Ruiter GCW, Wang HA, Knight AM, Spinner RJ, Yaszemski MJ, Windebank AJ, Pandit A (2010) Controlling dispersion of axonal regeneration using a multichannel collagen nerve conduit. *Biomaterials* 31:5789–5797
- Bagher Z, Azami M, Ebrahimi-Barough S, Mirzadeh H, Solouk A, Soleimani M, Ai J, Nourani MR, Joghataei MT (2016) Differentiation of Wharton's Jelly-derived mesenchymal stem cells into motor neuron-like cells on three-dimensional collagen-grafted nanofibers. *Mol Neurobiol* 53:2397–2408
- Li CW, Davis B, Shea J, Sant H, Gale BK, Agarwal J (2018) Optimization of micropatterned poly(lactic-co-glycolic acid) films for enhancing dorsal root ganglion cell orientation and extension. *Neural Regen Res* 13:105–111
- Dalby MJ, Riehle MO, Yarwood SJ, Wilkinson CDW, Curtis ASG (2003) Nucleus alignment and cell signaling in fibroblasts: response to a micro-grooved topography. *Exp Cell Res* 284:274–282
- Hsu SH, Lu PS, Ni HC, Su CH (2007) Fabrication and evaluation of microgrooved polymers as peripheral nerve conduits. *Biomed Microdevice* 9:665–674
- Goldner JS, Bruder JM, Li G, Gazzola D, Hoffman-Kim D (2006) Neurite bridging across micropatterned grooves. *Biomaterials* 27:460–472

23. George JH, Nagel D, Waller S, Hill E, Parri HR, Coleman MD, Cui ZF, Ye H (2018) A closer look at neuron interaction with track-etched microporous membranes. *Sci Rep* 8:1–11
24. Teo BKK, Ankam S, Chan LY, Yim EKF (2010) Nanotopography/mechanical induction of stem-cell differentiation. *Nuclear Mech Genome Regul* 98:241–294
25. Nguyen AT, Sathe SR, Yim EKF (2016) From nano to micro: topographical scale and its impact on cell adhesion, morphology and contact guidance. *J Phys Condens Matter* 28:183001
26. Simitzi C, Karali K, Ranella A, Stratakis E (2018) Controlling the outgrowth and functions of neural stem cells: the effect of surface topography. *Chem Phys Chem* 19:1143–1163
27. Chua JS, Chng CP, Moe AAK, Tann JY, Goh ELK, Chiam KH, Yim EKF (2014) Extending neurites sense the depth of the underlying topography during neuronal differentiation and contact guidance. *Biomaterials* 35:7750–7761
28. Roach P, Parker T, Gadegaard N, Alexander MR (2010) Surface strategies for control of neuronal cell adhesion: a review. *Surf Sci Rep* 65:145–173
29. Tonazzini I, Meucci S, Van Woerden GM, Elgersma Y, Cecchini M (2016) Impaired Neurite contact guidance in ubiquitin ligase E3a (Ube3a)-deficient hippocampal neurons on nanostructured substrates. *Adv Healthc Mater* 5:850–862
30. Togari A, Dickens G, Kuzuya H, Guroff G (1985) The effect of fibroblast growth-factor on Pc12 cells. *J Neurosci* 5:307–316
31. Li RX, Kong Y, Ladisch S (1998) Nerve growth factor-induced neurite formation in PC12 cells is independent of endogenous cellular gangliosides. *Glycobiology* 8:597–603
32. Vaudry D, Stork PJS, Lazarovici P, Eiden LE (2002) Signaling pathways for PC12 cell differentiation: making the right connections. *Science* 296:1648–1649
33. Kuang SK, Yang X, Wang Z, Huang T, Kindy M, Xi T, Gao BZ (2016) How microelectrode array-based chick forebrain neuron biosensors respond to glutamate NMDA receptor antagonist AP5 and GABAA receptor antagonist musimol. *Sens Bio-Sens Res* 10:9–14
34. Fjellidal MF, Freyd T, Evenseth LM, Sylte I, Ring A, Paulsen RE (2019) Exploring the overlapping binding sites of ifenprodil and EVT-101 in GluN2B-containing NMDA receptors using novel chicken embryo forebrain cultures and molecular modeling. *Pharmacol Res Perspect* 7:e00480
35. Foley JD, Grunwald EW, Nealey PF, Murphy CJ (2005) Cooperative modulation of neuritogenesis by PC12 cells by topography and nerve growth factor. *Biomaterials* 26:3639–3644
36. Tian LL, Prabhakaran MP, Hu J, Chen ML, Besenbacher F, Ramakrishna S (2016) Synergistic effect of topography, surface chemistry and conductivity of the electrospun nanofibrous scaffold on cellular response of PC12 cells. *Colloids Surf B* 145:420–429
37. Erdman NR (2016) Creation of a pioneer-neuron axonal pathfinding model for future use in developmental neurotoxicity testing applications, Ph.D. Thesis, Clemson University, United State
38. Pettmann B, Louis JC, Sensenbrenner M (1979) Morphological and biochemical maturation of neurones cultured in the absence of glial cells. *Nature* 281:378–380
39. Arfsten J, Bradtmoller C, Kampen I, Kwade A (2008) Compressive testing of single yeast cells in liquid environment using a nanoindentation system. *J Mater Res* 23:3153–3160
40. Ahmad MR, Nakajima M, Kojima S, Homma M, Fukuda T (2010) Nanoindentation methods to measure viscoelastic properties of single cells using sharp, flat, and buckling tips inside esem. *IEEE Trans Nanobiosci* 9:12–23
41. Kuznetsova TG, Starodubtseva MN, Yegorenkov NI, Chizhik SA, Zhdanov RI (2007) Atomic force microscopy probing of cell elasticity. *Micron* 38:824–833
42. Seidlits SK, Khaing ZZ, Petersen RR, Nickels JD, Vanscoy JE, Shear JB, Schmidt CE (2010) The effects of hyaluronic acid hydrogels with tunable mechanical properties on neural progenitor cell differentiation. *Biomaterials* 31:3930–3940
43. Qian J, Wang J, Gao H (2008) Lifetime and strength of adhesive molecular *bond* clusters between elastic media. *Langmuir* 24:1262–1270
44. Zhang WL, Lin Y, Qian J, Chen WQ, Gao H (2013) Tuning molecular adhesion via material anisotropy. *Adv Func Mater* 23:4729–4738
45. Aeschlimann M (2000) Biophysical models of axonal pathfinding, Ph.D. Thesis, University of Lausanne, Switzerland
46. Yin J, Coutris N, Huang Y (2011) Investigation of inner surface groove formation under radially inward pressure during immersion precipitation-based hollow fiber membrane fabrication. *J Manufact Sci Eng Trans Asme* 133:587–626
47. Gong Z (2017) Physical understanding of cells and cell-ECM interactions, Ph.D. Thesis, University of Hong Kong, Hong Kong SAR
48. Dennerll TJ, Joshi HC, Steel VL, Buxbaum RE, Heidemann SR (1988) Tension and compression in the cytoskeleton of Pc-12 neurites II—quantitative measurements. *J Cell Biol* 107:665–674
49. Kobayashi N, Mundel P (1997) A role of microtubules during the formation of cell processes in neuronal and nonneuronal cells. *Cell Tissue Res* 291:163–174
50. Kiddie G, McLean D, Van Ooyen A, Graham B (2005) Biologically plausible models of neurite outgrowth. *Prog Brain Res* 147:67–80
51. Yin J, Coutris N, Huang Y (2012) Numerical study of axonal outgrowth in grooved nerve conduits. *J Neural Eng* 9:056001
52. Raffa V, Falcone F, De Vincentiis S, Falconieri A, Calatayud MP, Goya GF, Cuschieri A (2018) Piconewton mechanical forces promote neurite growth. *Biophys J* 115:2026–2033
53. Kilinc D, Blasiak A, O’Mahony JJ, Lee GU (2014) Low piconewton towing of cns axons against diffusing and surface-bound repellents requires the inhibition of motor protein-associated pathways. *Sci Rep* 4:7128
54. Szymanski JM, Zhang KR, Feinberg AW (2017) Measuring the Poisson’s ratio of fibronectin using engineered nanofibers. *Sci Rep* 7:1–9
55. Ouyang H, Nauman E, Shi RY (2013) Contribution of cytoskeletal elements to the axonal mechanical properties. *J Biol Eng* 7:21
56. Fass JN, Odde DJ (2003) Tensile force-dependent neurite elicitation via anti-beta 1 integrin antibody-coated magnetic beads. *Biophys J* 85:623–636
57. Riggio C, Calatayud MP, Giannaccini M, Sanz B, Torres TE, Fernandez-Pacheco R, Ripoli A, Ibarra MR, Dente L, Cuschieri A, Goya GF, Raffa V (2014) The orientation of the neuronal growth process can be directed via magnetic nanoparticles under an applied magnetic field. *Nanomed Nanotechnol Biol Med* 10:1549–1558
58. O’Toole M, Lamoureux P, Miller KE (2008) A Physical model of axonal elongation: force, viscosity, and adhesions govern the mode of outgrowth. *Biophys J* 94:2610–2620
59. Hoffman-Kim D, Mitchel JA, Bellamkonda RV (2010) Topography, Cell response, and nerve regeneration. *Annu Rev Biomed Eng* 12:203–231
60. Omotade OF, Pollitt SL, Zheng JQ (2017) Actin-based growth cone motility and guidance. *Mol Cell Neurosci* 84:4–10
61. Lowery LA, Van Vactor D (2009) The trip of the tip: understanding the growth cone machinery. *Nat Rev Mol Cell Biol* 10:332–343
62. Abe K, Katsuno H, Toriyama M, Baba K, Mori T, Hakoshima T, Kanemura Y, Watanabe R, Inagaki N (2018) Grip and slip of L1-CAM on adhesive substrates direct growth cone haptotaxis. *Proc Natl Acad Sci USA* 115:2764–2769

63. Li NZ, Folch A (2005) Integration of topographical and biochemical cues by axons during growth on microfabricated 3-D substrates. *Exp Cell Res* 311:307–316
64. Goriely A, Budday S, Kuhl E (2015) *Neuromechanics: from Neurons to Brain*. *Adv Appl Mech* 48:79–139
65. Balaban NQ, Schwarz US, Riveline D, Goichberg P, Tzur G, Sabanay I, Mahalu D, Safran S, Bershadsky A, Addadi L, Geiger B (2001) Force and focal adhesion assembly: a close relationship studied using elastic micropatterned substrates. *Nat Cell Biol* 3:466–472
66. Sarangi BR, Gupta M, Doss BL, Tissot N, Lam F, Mege RM, Borghi N, Ladoux B (2017) Coordination between intra- and extracellular forces regulates focal adhesion dynamics. *Nano Lett* 17:399–406
67. Goodno BJ, Gere JM (2018) *Mechanics of materials*, 9th edn. Cengage Learning, Boston
68. Beer FP, Johnston ER Jr, DeWolf JT, Mazurek DF (2017) *Statics and mechanics of materials*, 2nd edn. McGraw-Hill Education, New York
69. Gao HJ, Qian J, Chen B (2011) Probing mechanical principles of focal contacts in cell-matrix adhesion with a coupled stochastic-elastic modelling framework. *J R Soc Interface* 8:1217–1232